Research Article

Cross-Species Bioinspired Anisotropic Surfaces for Active Droplet Transportation Driven by Unidirectional Microcolumn Waves

Yuegan Song,[§] Shaojun Jiang,[§] Guoqiang Li,* Yachao Zhang, Hao Wu, Cheng Xue, Hongshu You, Dehu Zhang, Yong Cai, Jiangong Zhu, Wulin Zhu, Jiawen Li, Yanlei Hu,* Dong Wu, and Jiaru Chu

Cite This: ACS Appl. Mater. Interfaces 2020, 12, 42264−42273

Read Online

ACCESS | Metrics & More | Article Recommendations | Supporting Information

ABSTRACT: Natural evolution has endowed diverse species with distinct geometric micro/nanostructures exhibiting admirable functions. Examples include anisotropic microgrooves/microstripes on the rice leaf surface for passive liquid directional rolling, and motile microcilia widely existed in mammals' body for active matter transportation through in situ oscillation. Till now, bionic studies have been extensively performed by imitating a single specific biologic functional system. However, bionic fabrication of devices integrating multispecies architectures is rarely reported, which may sparkle more fascinating functionalities beyond natural findings. Here, a cross-species design strategy is adopted by combining the anisotropic wettability of the rice leaf surface and the directional transportation characteristics of motile cilia. High-aspect-ratio magnetically responsive microcolumn array (HAR-MRMA) is prepared for active droplet transportation. It is found that just like the motile microcilia, the unidirectional waves are formed by the real-time reconstruction of the microcolumn array under the moving magnetic field, enabling droplet (1−6 μL) to transport along the predetermined anisotropic orbit. Meanwhile, on-demand droplet horizontal transportation on the inclined plane can be realized by the rice leaf-like anisotropic surface, showcasing active nongravity-driven droplet transportation capability of the HAR-MRMA. The directional lossless transportation of droplet holds great potential in the fields of microfluidics, chemical microreaction, and intelligent droplet control system.

KEYWORDS: high-aspect ratio, magnetically responsive, unidirectional waves, anisotropic properties, directional transportation
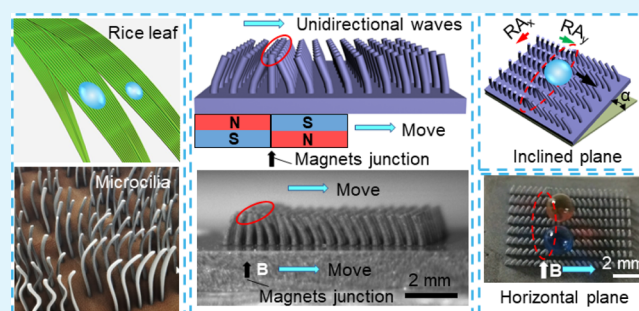
1. INTRODUCTION

To survive in the washy environment, rice leaves have evolved the ability to transport droplets directionally and efficiently with the aid of anisotropic surface microgrooves.[1,2] Recently, the excellent anisotropic wettability of rice leaves has been attracting considerable interests.[3−6] For example, inspired by the microgroove of rice leaf, directional oil sliding surfaces were realized with hierarchical anisotropic groove microstructures.[7] Groove-like microstructures were fabricated on cooper surfaces to study the influence of anisotropic groove microstructures on the wettability and sliding behavior of water droplet.[8] Synthetic rice leaf-like wavy surfaces with tunable anisotropic wettability were prepared to investigate the effects of the hierarchical nanostructure surface roughness on the anisotropic wettability and water repellency.[9] A smart superhydrophobic surface with shape memory materials was realized, on which the wetting performances can be switched reversibly between the superhydrophobic isotropic and anisotropic states.[10]

In addition, motile cilia widely exists in animals[11,12] and can realize the directional transportation of matter in an active manner by oscillating in a certain direction.[13,14] Inspired by

motile cilia, researchers have designed dynamic functional surface structures, which can respond to external stimuli to achieve important functions.[15−18] For example, based on the airway cilium-like magnetically responsive conical arrays, nonmagnetic polystyrene microspheres can be transported directionally and continuously by the bending and recovering of conical arrays.[19] Droplets can be transported on the superhydrophobic magnetic microcilia array prepared by combining the template and superhydrophobic nanosilica-n-hexane modification, and the rolling/pinning states can be switched on the inclined surface by the magnetic field with the aid of gravity.[20] A functional surface with anisotropic slippery switchable microstructures was prepared, on which droplets can preferentially slip and spread against the direction of cilia tilt under gravity.[21]
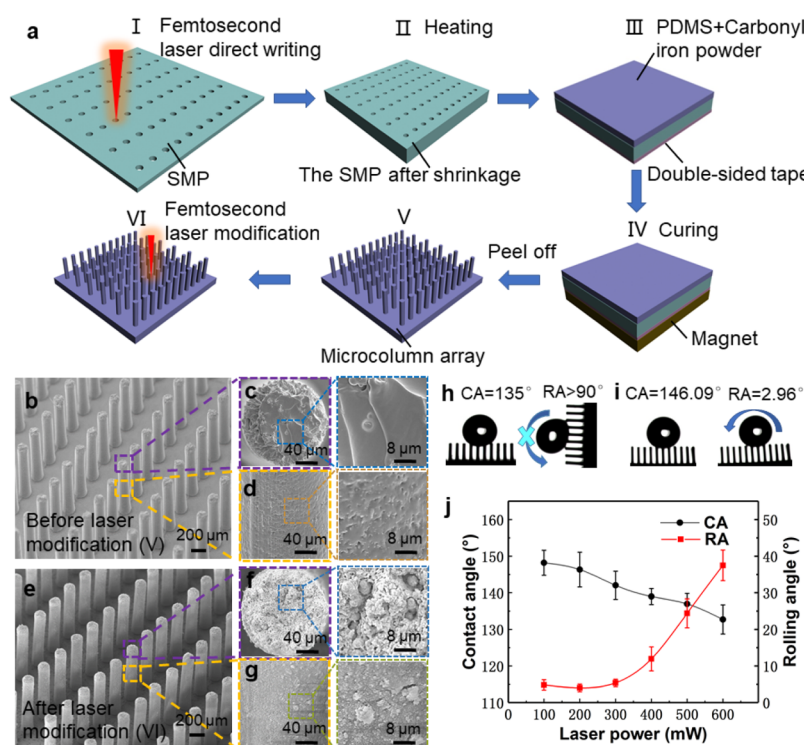
Figure 1. Fabrication of the HAR-MRMA and surface properties before and after laser modification. (a) Schematic illustration of the fabrication procedure of HAR-MRMA. (b−g) Scanning electron microscopy images of HAR-MRMA before and after laser modification. Contact angle and rolling angle (h) before laser modification and (i) after laser modification. (j) Quantitative relationship between the contact angle and rolling angle of the HAR-MRMA after laser modification with different laser powers. The droplet volume used here is 4 μL.

It can be found that the current studies on the anisotropy of rice leaf surface are basically focused on passive droplet transportation,[22−26] which always depends on gravity to make the droplets roll away.[27,28] Furthermore, although droplet manipulation on the inclined plane has been achieved under gravity,[20,21,29−31] the gravity-free droplet horizontal transportation on the inclined plane has not been studied. Besides, it is of great significance to realize directional active transportation of droplet on the cilia-like surface. Therefore, it is highly desirable to realize directional active droplet transportation combining the biological structure characteristics of the rice leaf surface and motile cilia.

Herein, a cross-species bionic design strategy is adopted for constructing active anisotropic droplet transportation surfaces, which combines the anisotropic wettability of rice leaf surface and the directional transportation characteristics of motile cilia. The surface consists of high-aspect ratio magnetically responsive microcolumn array (HAR-MRMA) prepared by femtosecond laser direct writing and soft transfer technology,[32,33] so that controlled directional and nondestructive transportation of droplets is driven by external magnetic field. The mechanism is that droplet can be directionally propelled by the unidirectional waves, which are formed by the real-time reconstruction of the microcolumn array under the moving magnetic field.[34,35] In addition, because of the rice leaf-like anisotropy of the HAR-MRMA, the droplet can move horizontally on the inclined surface, which is difficult to realize by other cilia-like structures.[19−21,29,30] This cross-species-combined bionic HAR-MRMA paves a new way for the study of droplet manipulation and directional lossless transportation.[21,22,36]

2. RESULTS AND DISCUSSION

2.1. Principle and Preparation Process of HAR-MRMA. The principle and preparation process of HAR-MRMA are shown in Figure 1a. High-aspect ratio microhole array is fabricated on the shape memory polystyrene (SMP) polymer surface using the thermal shrinkage property (Figures S1 and S2, Supporting Information).[37] First, the microhole array is fabricated on the SMP by femtosecond laser direct drilling (Figure 1a, I).[38,39] In order to introduce anisotropy into the microhole array, the distances between adjacent microholes in the transverse and longitudinal directions are designed to be different. Also, then, the SMP sheet with microhole array is heated in an oven at 130 °C for 10 min for complete shrinkage (Figure S3−S5, Supporting Information). After shrinkage, the thickness of the polystyrene film increases from initial ∼150 μm to final ∼1014 μm (Figure S6, Supporting Information), and the length and width are contracted to ∼40% of the original size (Figure 1a, II). As a result, the microhole array with a high-aspect ratio can be simply prepared. Then, the polydimethylsiloxane (PDMS) doped with carbonyl iron powder is cast into the shrunk polystyrene film to obtain the microcolumn structures (transfer process) (Figure 1a, III, Figure S7, Supporting Information). Here, double-sided tape is stuck to one side of the shrunk polystyrene sheet to prevent the PDMS from leaking.

In order to ensure a larger bending degree of the microcolumn under the magnetic field, a piece of neodymium−iron−boron (NdFeB) magnet (40 × 40 × 20 mm) is placed under the sample about 8 s, so that the iron particles in the microcolumns are arranged into chains.[40] After curing in an oven at 130 °C for 20 min (Figure 1a, IV), the double-sided tape is removed carefully to expose the polystyrene mold.
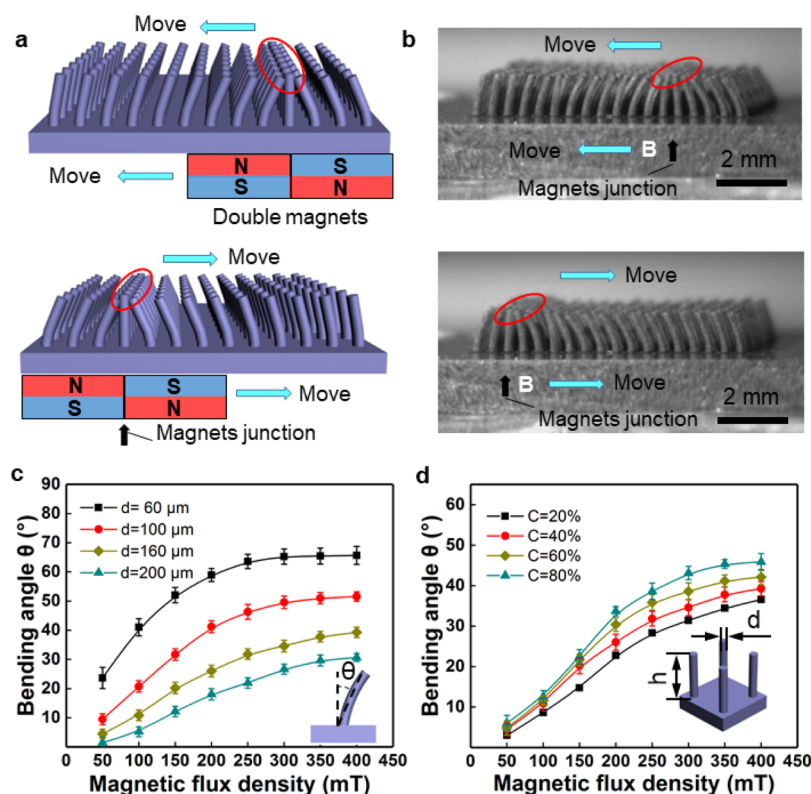
Figure 2. Magnetically responsive bending properties of HAR-MRMA. (a) Three-dimensional models of unidirectional waves of HAR-MRMA under magnetic field. (b) Optical image of the response of microcolumns to the magnetic field. (c) Quantitative relationship between the magnetic flux density and the bending angle of the microcolumns with different diameters and the constant iron powder concentrations (C = 40%). (d) Quantitative relationship between the magnetic flux density and the bending angle of the microcolumns with the different iron powder concentrations (C) C = 20%, C = 40%, C = 60%, and C = 80%, respectively. The diameter of the microcolumns is d = 160 μm. h remains to be 1014 μm.

Subsequently, the superhydrophobic microcolumn array with high adhesion to droplet is stripped out of the mold (Figure 1a, V). Finally, after femtosecond laser modification, the achieved HAR-MRMA surface is changed to be superhydrophobic with low adhesion (Figure 1a, VI).

As shown in Figure 1b−g, before laser scanning, the central part of microcolumns is relatively smoother than the edge region because of the contact between the top of microcolumn and double-sided tape. After laser scanning, it can be seen that the top of microcolumns is evenly covered by rough micronanostructures while the side walls of the microcolumns are deposited with a few micronanoparticles (Figure S8, Supporting Information). These micronanostructures are generated by laser ablation with vertically crossed scanning and the deposition of broken particles during ablation. In other words, micronanostructures with different roughnesses are induced after femtosecond laser modification (Figure S9, Supporting Information). It should be noted that after laser modification, the crystal structure of each component of HAR-MRMA is not changed, and there is no visible chemical composition change on the surface (Figure S7, Supporting Information). As shown in Figure 1h, the initial contact angle (CA) of untreated HAR-MRMA is about 135°. When the sample is rotated to be vertical, the droplet cannot fall down, demonstrating high surface adhesion. Figure 1i shows the wetting properties of HAR-MRMA after femtosecond laser modification. The CA is about 146.09°, and the rolling angle (RA) is significantly reduced to 2.96°.[41] Based on the Cassie equation,[42] the surface adhesion is reduced with the decrease of contact area of solid/liquid interface. The rough surface makes the HAR-MRMA surface become superhydrophobic low adhesion. The relationships between laser power and CA/RA values are shown in Figure 1j. It can be clearly seen that with the increase of laser power, the CA decreases and the RA increases. The reason is that more hydrophilic iron powders are exposed to the surface of structure with the increase of laser power.

2.2. Magnetic Response Properties of HAR-MRMA. In order to study the magnetic response properties of HAR-MRMA, two connected square NdFeB permanent magnets are placed at the bottom of the sample (Figure 2a). It can be observed that the real-time reconstruction of microcolumn array on the HAR-MRMA surface can form a unidirectional wave under magnetic driving force, and the unidirectional wave is located above the junction between the two magnets. When the magnets move from right to left, the unidirectional wave formed by the microcolumns also moves from right to left. Correspondingly, unidirectional waves move from left to right with the right moving of the magnets under the action of magnetic field. Figure 2b shows optical images of the microcolumns responding to the magnetic field (Video S1, Supporting Information). There is good reversibility and repeatability of the bending behavior of HAR-MRMA under magnetic field (Video S2, Supporting Information).

Considering the close relationship between the bending behavior of the HAR-MRMA and the droplet transportation capacity,[43] the maximum bending degree of the microcolumns is studied under different magnetic flux densities (B). The
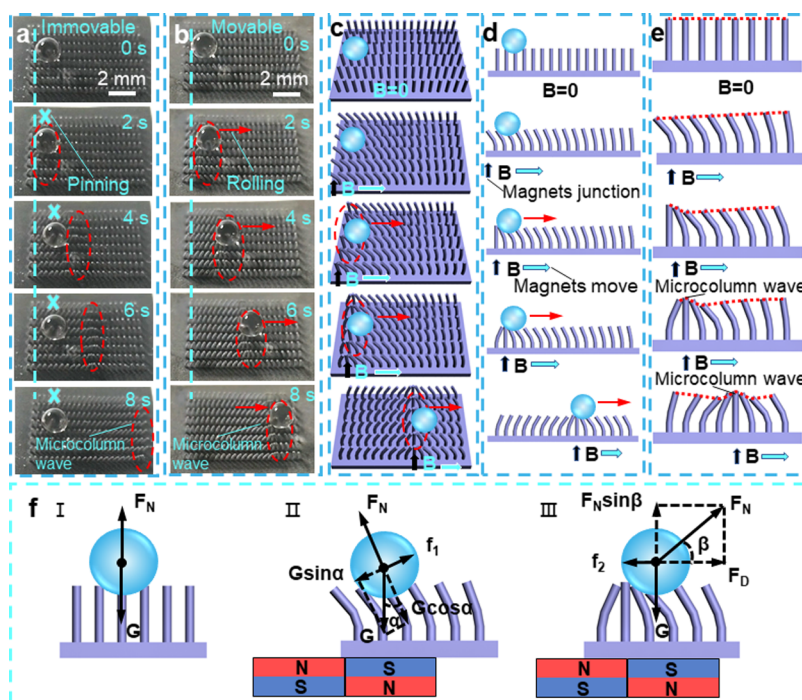
Figure 3. Analysis of droplet transportation mechanism on the HAR-MRMA surface. Optical images of droplet transportation on the HAR-MRMA (a) before laser modification and (b) after laser modification. (c) Three-dimensional model illustration of droplet transportation on the HAR-MRMA after laser modification. (d) Side-view models of droplet transportation on the HAR-MRMA surface. (e) Schematic illustration of formation mechanism of unidirectional waves on the HAR-MRMA surface. (f) Analysis of the mechanism of droplet transportation on the HAR-MRMA surface.

magnitude of magnetic flux density was controlled by changing the vertical distance between the microcolumn array and magnet (Figure S10, Supporting Information). To avoid the interaction between microcolumns, a single row of micro-columns is selected in the sample. As shown in Figure 2c, the diameter of the microcolumns is changed from 60 to 100 μm, 160, and 200 μm. When the iron powder concentrations (C) are 40%, the bending angle increases with the magnetic flux density. When the magnetic flux density is constant, the bending angle increases with the decrease of the microcolumn diameter (d). As shown in Figure 2d, with the same microcolumn diameter (d = 160 μm) and iron powder concentrations, the bending angle increases with the magnetic flux density (Figure S11, Supporting Information, d = 120 μm). Furthermore, the bending angle increases with the iron powder concentrations (C = 20%, C = 40%, C = 60%, and C = 80%, respectively) with the same microcolumn diameter (160 μm) and magnetic flux density.

2.3. Mechanism for Droplet Transportation on the HAR-MRMA. Figure 3a shows droplet transportation on the HAR-MRMA before femtosecond laser modification, and it indicates that the unidirectional wave can form under the magnetic response. However, the unidirectional wave does not exert enough force to drive the droplet because of the strong adhesion between the droplet and the top of microcolumns. In contrast, the droplet on the femtosecond laser-modified HAR-MRMA surface can be transported unidirectionally by the unidirectional wave because of the low adhesion force (Figure 3b, Video S3, Supporting Information).

It is necessary to analyze the transportation mechanism of droplet on the low-adhesion superhydrophobic HAR-MRMA surface. As shown in Figure 3c−e, when the magnetic flux density is zero, the microcolumns remain upright, and the

droplet is in equilibrium. When two joined magnets (The N and S poles are distributed up and down.) are placed under the microcolumn array, the microcolumn always bend toward the junction of two magnets. It should be noted that the microcolumn, which locates exactly above the junction, remains upright. With the magnet movement from left to right, the bending direction of microcolumns is changed from left to right, resulting in the real-time reconstruction of the microcolumn array to form the continuous unidirectional waves. Thus, the equilibrium state of the droplet is broken, and the droplet is transported.

As shown in Figure 3f, the droplet transportation process can be divided into three steps. When the magnetic flux density is zero (Figure 3f step I), the gravity (G) of the droplet is equal to the surface supporting force (F_N). When applying two external magnets (step II), the motion-less state of droplet can be described by eqs 1 and 2 as follows

$$f_1 = G \sin \alpha \tag{1}$$

$$F_N = G \cos \alpha \tag{2}$$

where α is the angle between gravity and normal force F_N, f_1 is the frictional force that prevents the droplet from rolling to the left, $G \sin \alpha$ is the component force of gravity along the direction of frictional force, and $G \cos \alpha$ is the component force of gravity along the direction of normal force. The third state is shown in Figure 3f, III. With the movement of magnets from left to right, the droplet is in an inequilibrium state, which can be described by the following eq 3

$$F_D = F_N \cos \beta > f_2 \tag{3}$$

where F_D is the driving force from the bent microcolumn, β is the angle between normal force F_N and driving force F_D, and f_2
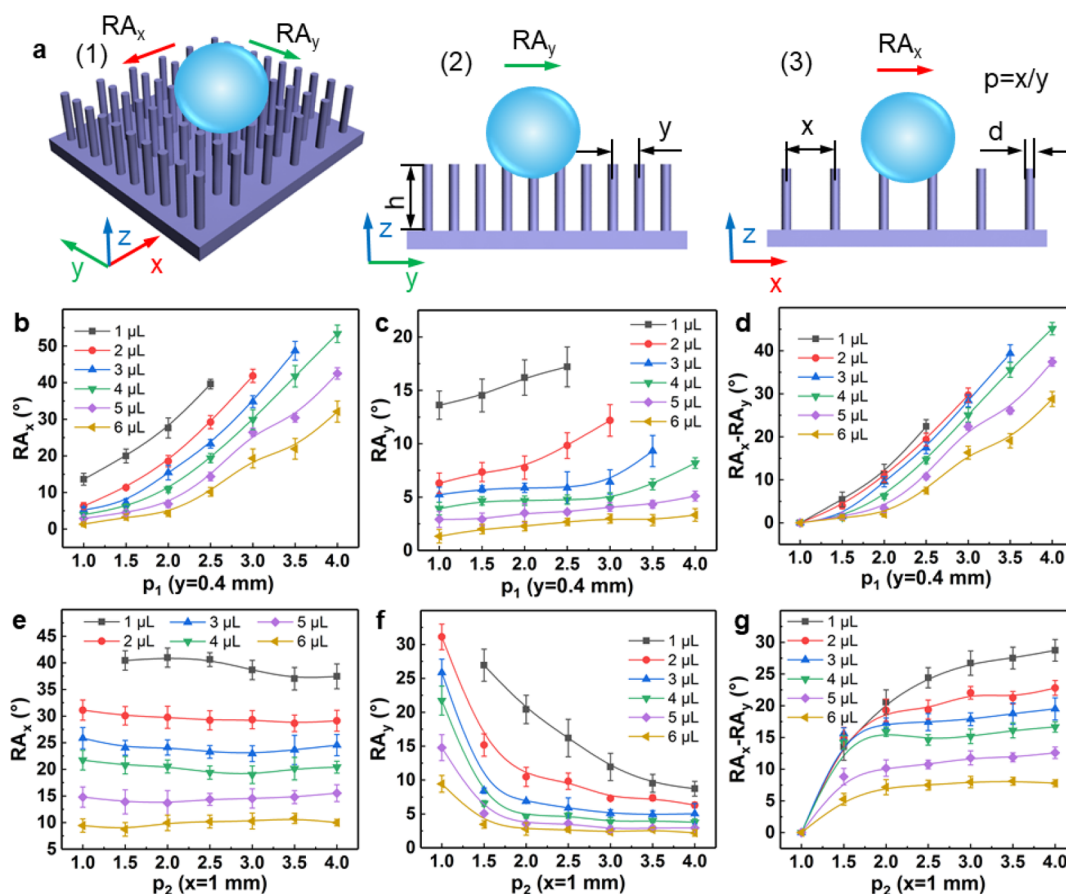
Figure 4. Anisotropic properties of droplets on the HAR-MRMA surface. (a) Illustration of RAs of droplet along the X axis (RA$_x$) and Y axis (RA$_y$) on the HAR-MRMA surface. Quantitative relationships between (b) p_1 and RA$_x$, (c) p_1 and RA$_y$, (d) p_1 and RA difference (RA$_x$ − RA$_y$), (e) p_2 and RA$_x$, (f) p_2 and RA$_y$, and (g) p_2 and RA difference (RA$_x$ − RA$_y$).

is the frictional force between the droplet and microcolumn surface. Under the resulting net forces, the droplet will move right on the HAR-MRMA surface.

2.4. Anisotropic Properties of Droplets on the HAR-MRMA Surface. In order to study the influence of the anisotropy on droplet transportation performance, the isotropic HAR-MRMA surface is prepared as a control group. By comparing the effects of isotropic and anisotropic HAR-MRMA surfaces on the droplet transportation, it has been proved that the droplet can be transported directionally and stably on the anisotropic HAR-MRMA surface rather than the isotropic HAR-MRMA surface (Video S4, Supporting Information), indicating that anisotropic properties of HAR-MRMA play an essential role in the droplet transportation.

The RAs of droplet along the X axis (RA$_x$) and Y axis (RA$_y$) are shown in Figure 4a. The interval ratio p is defined as the ratio between the microcolumn intervals in two orthogonal directions: x/y (x and y are the distance between the microcolumns along the X axis and the Y axis). As shown in Figure 4b,c, with the same droplet volume, RA$_x$ and RA$_y$ increase with p_1 (y = 0.4 mm, x changes to be 0.4, 0.6, 0.8, 1, 1.2, 1.4, and 1.6 mm). When the droplet volume is 1 μL, the RA of droplet cannot be measured with p_1 = 3.0, 3.5 and 4.0. The reason is that the droplet gets into the groove of the microcolumns. Furthermore, 2 μL of droplet can be stuck in the groove when p_1 = 3.5 and 4.0. As shown in Figure 4d, the difference between RA$_x$ and RA$_y$ increases with p_1. It means that with the increase of p_1, the transportation of droplet is

more stable. However, if p_1 is too large, the small droplet cannot be transported. Therefore, p_1 is an important factor for droplet transportation.

Similarly, the relationship between p_2 (x/y, x = 1 mm) and droplet RA is studied. When y is changed from 0.25 to 0.286, 0.332, 0.4, 0.5, 0.668, and 1 mm, the quantitative relationship between p_2 and RA$_x$/RA$_y$ is shown in Figure 4e,f. With the same droplet volume, RA$_x$ remains almost unchanged with p_2 (x = 1 mm). Furthermore, RA$_y$ decreases as p_2 increases. As one can see in Figure 4g, the difference between RA$_x$ and RA$_y$ increases with p_2 under the same droplet volume, and the droplet transportation is more stable. When the droplet volume (V) > 2 μL and $p_2 \geq 2$, the difference between RA$_x$ and RA$_y$ is almost constant. Therefore, p_2 is chosen to be 2 so as to achieve stable transportation of small droplet.

2.5. Stability of Droplet Transportation on the HAR-MRMA Surface. The anisotropic design of HAR-MRMA surface is one of the key factors for droplet stable transportation. Stable transportation means that the droplet can move along a specified orbit or stop on demand under the driving of the unidirectional waves. Correspondingly, unstable transportation means that the droplet may be bounced off or cannot roll, or the droplet cannot be transported along the predesigned orbit.

Figure 5a shows the droplet transportation performance with varying microcolumn diameter (d) and droplet volume (V). When 60 μm $\leq d \leq$ 100 μm, the droplet cannot be transported stably, which is mainly caused by the small microcolumn
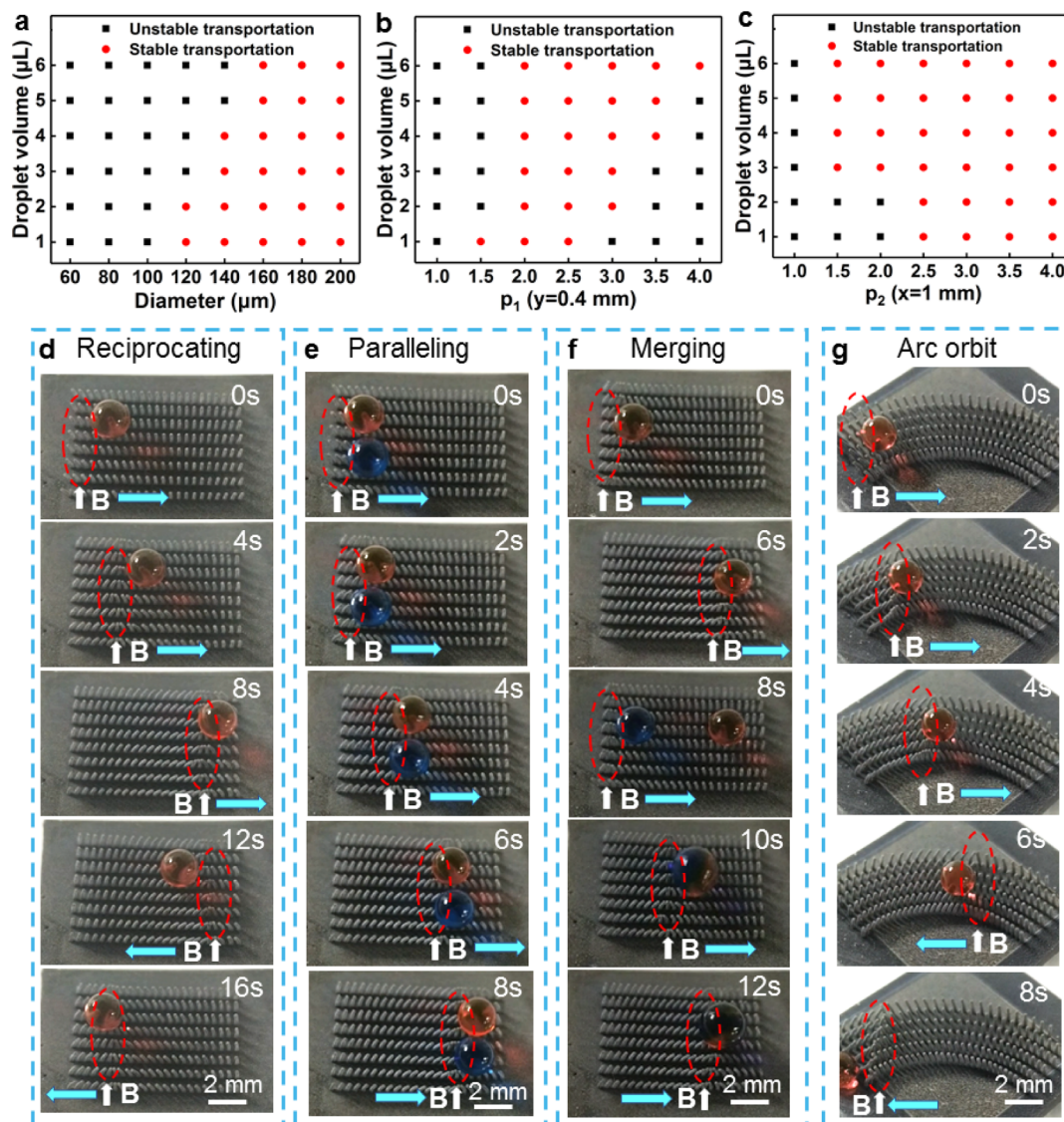
Figure 5. Droplet transportation stability on the HAR-MRMA surface. (a−c) Dependence of transportation performance on (a) the diameter of microcolumns and the volume of droplet, (b) p_1 and droplet volume, and (c) p_2 and droplet volume. (d−g) Diversified transportation modes of droplets on the HAR-MRMA surface. (d) Reciprocation of droplet along the straight orbit under magnetic field. (e) Two droplets moving in parallel. (f) Merging transportation of droplets and (g) directional stable transportation of droplet on circular arc orbit. The droplet volume is 3 μL. The spacing between microcolumns was x = 0.8 mm and y = 0.4 mm, and the magnetic flux density (B) is 200 ± 10 mT.

diameter resulting in large bending angle and uneven bending degree. When d = 120 μm, only the droplet with smaller volumes of 1 and 2 μL can be transported. When d = 140 μm, the droplet with a volume of 1−4 μL can be transported stably. When d = 160, 180, and 200 μm, droplets (1−6 μL) can be transported stably.

Figure 5b shows the dependence of droplet transportation performance on p_1 and droplet volume. When p_1 = 1, the droplet (1−6 μL) cannot be transported stably on HAR-MRMA surface because of the isotropic surface. When p_1 = 1.5, only droplet with a volume of 1 μL can be transported. When p_1 = 2.0 and 2.5, the droplet (1−6 μL) can be transported stably because of anisotropic design (Video S5, Supporting Information). When $p_1 \geq 3$, small droplets cannot be transported because they get stuck in the groove. Similarly, as shown in Figure 5c, when p_2 = 1, the droplet (1−6 μL) cannot be transported either. When p_2 = 1.5 and p_2 = 2, large droplet (3−6 μL) can be transported. When p_2 = 2.5, p_2 = 3.0,

p_2 = 3.5, and p_2 = 4.0, the droplet (1−6 μL) can all be transported. The results indicate that the distance between the microcolumns along the X axis (x) has a significant influence on the droplet transportation while the distance between the microcolumns along the Y axis (y) has no obvious influence on droplet transportation.

Subsequently, the droplet transportation properties on the horizontal HAR-MRMA surface are demonstrated. Figure 5d shows the reciprocation of droplet along the straight orbit propelled by the unidirectional waves. Two droplets moving in parallel are shown in Figure 5e. Two droplets are placed onto the HAR-MRMA surface and then propelled parallelly from left to right. The merging transportation of two droplets is shown in Figure 5f. The red droplet is first transported to right, and then, the blue droplet is added to the starting position to propel toward the red one and merge with it. Figure 5g shows that droplet can be transported stably along the circular arc orbit under magnetic field (Video S6, Supporting Informa-
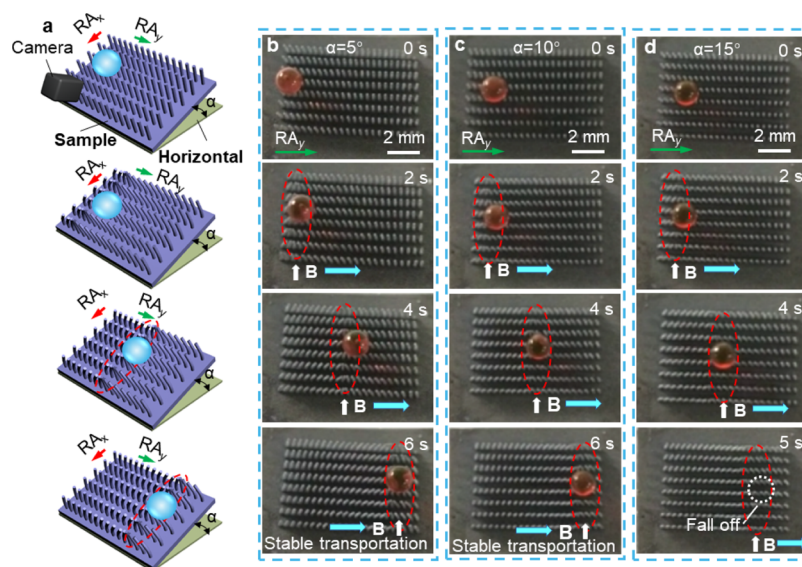
Figure 6. Droplet horizontal transportation on the anisotropic inclined plane. (a) Three-dimensional models of droplet horizontal transportation on the inclined plane. Droplet horizontal transportation on the inclined plane with the angle (α) (b) $\alpha = 5°$, (c) $\alpha = 10°$, and (d) $\alpha = 15°$. (b,c) Droplet is transported stably and (d) the droplet falls off after moving for 4 s. The spacing between the microcolumns is $x = 0.8$ mm and $y = 0.4$ mm, and the magnetic flux density (B) is 200 ± 10 mT.

tion). In addition, the directional stable transportation of droplet with different temperatures and pH is also realized on the HAR-MRMA surface (Figures S12−S14, Supporting Information).

The ingenious design of structure combining the anisotropic characteristics of microgrooves and the active oscillation of motile microcilia can not only realize the directional and lossless stable transportation of droplet on the horizontal plane but also meet the horizontal transportation requirements on the inclined plane. As shown in Figure 6, owing to the anisotropic design of the HAR-MRMA, the droplet can be transported on the inclined plane in the horizontal direction. Figure 6a shows the three-dimensional (3D) model diagram of droplet transportation on the inclined plane, and the droplet is driven along the RA$_y$ direction. Figure 6b,c shows that the droplet (2 μL) can be transported stably along the orbit on the inclined plane when the inclination angle is $\alpha = 5°$ and $\alpha = 10°$. When $\alpha = 15°$ (Figure 6d), the droplet falls off after moving for 4 s. All these results have proved that the anisotropic HAR-MRMA structure makes the horizontal transportation of droplet possible on the inclined plane because of different energy barriers along two directions (Video S7, Supporting Information).

3. CONCLUSIONS

In conclusion, inspired by the anisotropic wettability of rice leaf surface and the directional transportation characteristics of motile cilia, a kind of anisotropic droplet transportation surface HAR-MRMA is fabricated to achieve active directional and nondestructive transportation of droplets. The HAR-MRMA surface inherits the advantages of anisotropic transportation properties from rice leaf and active directional characteristics from motile microcilia. Because of the anisotropic design of the HAR-MRMA, multifunctional droplet transportation is realized including reciprocating motion in straight lines along the orbit, parallel movement, and merging of two droplets and directional stable transportation of droplet on circular arc orbit. Moreover, the HAR-MRMA surface can enable the droplet

horizontal transportation on the inclined plane, which is challenging for other cilia-like structures. The directional lossless transportation of droplet holds great potential in the fields of microfluidic control, chemical microreaction, and intelligent droplet control.

4. EXPERIMENTAL SECTION

4.1. Fabrication of HAR-MRMA. High-aspect ratio microhole array can be first prepared on the shape memory polymer (Hebei Pod network technology co., LTD surface) by femtosecond laser direct writing. Afterward, the SMP sheet with microhole array is heated for complete shrinkage. Then, the liquid PDMS and hardening agent (Sylgard 184, Dow Corning) in a weight ratio of 10:1 doped with carbonyl iron powder (diameter of 3−5 μm, purity ≥99.9%, $C = 40\%$, RuiTeng Alloy Material co., LTD) are cast into the shrinkage polystyrene film (transfer process) and degassed. Also, then, after curing in an oven (130 °C, 20 min), the microcolumn array was peeled off from the mold. Finally, the HAR-MRMA surface was obtained after femtosecond laser modification.

4.2. Instrument and Characterization. Microholes are processed on a SMP polymer by femtosecond laser direct writing technology. The laser beam (104 fs, 1 kHz, 800 nm) is from a regenerative-amplified Ti: sapphire femtosecond laser system (Legend Elite-1K-HE, Coherent), and the power of laser is 200 mw, and the scanning speed is 30 mm/s. When the laser is applied to modify the surface. the spacing between lines is 15 μm. Scanning electronic microscopy images were taken by JSM-6700F, JEOL, Japan. The CAs of the droplet were measured using a contact angle system (CA100C, Innuo, China).

■ ASSOCIATED CONTENT

ⓢ Supporting Information

The Supporting Information is available free of charge at https://pubs.acs.org/doi/10.1021/acsami.0c10034.

Thermal shrinkage property of shape memory polystyrene (SMP) polymer, statistical tables of microhole diameter before and after shrinkage and shrinkage ratio of five samples, scanning electron microscopy (SEM) images of microhole array of the third sample before and after shrinkage, SEM images of microhole array of the

fourth sample before and after shrinkage, SEM images of microhole array of the fifth sample before and after shrinkage, SEM images of the thickness of shape memory polystyrene (SMP) polymer before and after shrinkage, X-ray diffraction (XRD) and Fourier Transform Infrared spectroscopy (FT-IR) characterization of PDMS, iron powder, and mixture of PDMS and iron powder before and after laser modification, SEM images with high resolution before and after laser modification, atomic force microscopy (AFM) images of HAR-MRMA surface before and after laser modification, measurement of the magnetic flux density magnitude, quantitative relationship between the magnetic flux density and the bending angle of the microcolumns with the different iron powder concentrations (C), directional stable transportation of droplet with different temperatures (T), directional stable transportation of acidic solution (HCl) with different pH values, and directional stable transportation of alkaline solution (NaOH) with different pH values (PDF)

Unidirectional waves formed under magnetic driving force (AVI)

Reversibility and circularity of bending behavior of HAR-MRMA at the magnetic field (AVI)

Droplet transportation on the HAR-MRMA before and after femtosecond laser modification (AVI)

Droplet transportation on the isotropic HAR-MRMA surface (AVI)

Droplet transportation of different volumes (AVI)

Diversified transportation modes of droplets on the HAR-MRMA surface (AVI)

Droplet horizontal transportation on the anisotropic inclined plane (AVI)

■ AUTHOR INFORMATION

Corresponding Authors

    Guoqiang Li − *School of Manufacturing Science and Engineering, Key Laboratory of Testing Technology for Manufacturing Process, Ministry of Education, Southwest University of Science and Technology, Mianyang 621010, China*; Email: guoqli@swust.edu.cn

    Yanlei Hu − *CAS Key Laboratory of Mechanical Behavior and Design of Materials, Key Laboratory of Precision Scientific Instrumentation of Anhui Higher Education Institutes, Department of Precision Machinery and Precision Instrumentation, University of Science and Technology of China, Hefei 230026, China*; orcid.org/0000-0003-1964-0043; Email: huyl@ustc.edu.cn

Authors

    Yuegan Song − *CAS Key Laboratory of Mechanical Behavior and Design of Materials, Key Laboratory of Precision Scientific Instrumentation of Anhui Higher Education Institutes, Department of Precision Machinery and Precision Instrumentation, University of Science and Technology of China, Hefei 230026, China; School of Manufacturing Science and Engineering, Key Laboratory of Testing Technology for Manufacturing Process, Ministry of Education, Southwest University of Science and Technology, Mianyang 621010, China*

    Shaojun Jiang − *CAS Key Laboratory of Mechanical Behavior and Design of Materials, Key Laboratory of Precision Scientific Instrumentation of Anhui Higher Education Institutes,*

    Department of Precision Machinery and Precision Instrumentation, University of Science and Technology of China, Hefei 230026, China

    Yachao Zhang − *CAS Key Laboratory of Mechanical Behavior and Design of Materials, Key Laboratory of Precision Scientific Instrumentation of Anhui Higher Education Institutes, Department of Precision Machinery and Precision Instrumentation, University of Science and Technology of China, Hefei 230026, China*

    Hao Wu − *CAS Key Laboratory of Mechanical Behavior and Design of Materials, Key Laboratory of Precision Scientific Instrumentation of Anhui Higher Education Institutes, Department of Precision Machinery and Precision Instrumentation, University of Science and Technology of China, Hefei 230026, China*

    Cheng Xue − *CAS Key Laboratory of Mechanical Behavior and Design of Materials, Key Laboratory of Precision Scientific Instrumentation of Anhui Higher Education Institutes, Department of Precision Machinery and Precision Instrumentation, University of Science and Technology of China, Hefei 230026, China*

    Hongshu You − *CAS Key Laboratory of Mechanical Behavior and Design of Materials, Key Laboratory of Precision Scientific Instrumentation of Anhui Higher Education Institutes, Department of Precision Machinery and Precision Instrumentation, University of Science and Technology of China, Hefei 230026, China*

    Dehu Zhang − *School of Manufacturing Science and Engineering, Key Laboratory of Testing Technology for Manufacturing Process, Ministry of Education, Southwest University of Science and Technology, Mianyang 621010, China*

    Yong Cai − *School of Manufacturing Science and Engineering, Key Laboratory of Testing Technology for Manufacturing Process, Ministry of Education, Southwest University of Science and Technology, Mianyang 621010, China*

    Jiangong Zhu − *School of Manufacturing Science and Engineering, Key Laboratory of Testing Technology for Manufacturing Process, Ministry of Education, Southwest University of Science and Technology, Mianyang 621010, China*

    Wulin Zhu − *CAS Key Laboratory of Mechanical Behavior and Design of Materials, Key Laboratory of Precision Scientific Instrumentation of Anhui Higher Education Institutes, Department of Precision Machinery and Precision Instrumentation, University of Science and Technology of China, Hefei 230026, China*

    Jiawen Li − *CAS Key Laboratory of Mechanical Behavior and Design of Materials, Key Laboratory of Precision Scientific Instrumentation of Anhui Higher Education Institutes, Department of Precision Machinery and Precision Instrumentation, University of Science and Technology of China, Hefei 230026, China*; orcid.org/0000-0003-3950-6212

    Dong Wu − *CAS Key Laboratory of Mechanical Behavior and Design of Materials, Key Laboratory of Precision Scientific Instrumentation of Anhui Higher Education Institutes, Department of Precision Machinery and Precision Instrumentation, University of Science and Technology of China, Hefei 230026, China*; orcid.org/0000-0003-0623-1515

    Jiaru Chu − *CAS Key Laboratory of Mechanical Behavior and Design of Materials, Key Laboratory of Precision Scientific Instrumentation of Anhui Higher Education Institutes, Department of Precision Machinery and Precision*

Instrumentation, University of Science and Technology of China, Hefei 230026, China; ● orcid.org/0000-0001-6472-8103

Complete contact information is available at:
https://pubs.acs.org/10.1021/acsami.0c10034

Author Contributions
§Y.S. and S.J. contributed equally to this work.

Notes
The authors declare no competing financial interest.

■ REFERENCES

(1) Wu, D.; Wang, J.-N.; Wu, S.-Z.; Chen, Q.-D.; Zhao, S.; Zhang, H.; Sun, H.-B.; Jiang, L. Three-Level Biomimetic Rice-Leaf Surfaces with Controllable Anisotropic Sliding. *Adv. Funct. Mater.* **2011**, *21*, 2927−2932.

(2) Kong, T.; Luo, G.; Zhao, Y.; Liu, Z. Bioinspired Superwettability Micro/Nanoarchitectures: Fabrications and Applications. *Adv. Funct. Mater.* **2019**, *29*, 1808012.

(3) Tie, L.; Guo, Z.; Liu, W. Anisotropic wetting properties on various shape of parallel grooved microstructure. *J. Colloid Interface Sci.* **2015**, *453*, 142−150.

(4) Radha, B.; Lim, S. H.; Saifullah, M. S. M.; Kulkarni, G. U. Metal hierarchical patterning by direct nanoimprint lithography. *Sci. Rep.* **2013**, *3*, 1078.

(5) Zhu, D.; Li, X.; Zhang, G.; Zhang, X.; Zhang, X.; Wang, T.; Yang, B. Mimicking the Rice Leaf—From Ordered Binary Structures to Anisotropic Wettability. *Langmuir* **2010**, *26*, 14276−14283.

(6) Sun, T.; Feng, L.; Gao, X.; Jiang, L. Bioinspired Surfaces with Special Wettability. *Acc. Chem. Res.* **2005**, *38*, 644−652.

(7) Kang, S. M.; Lee, C.; Kim, H. N.; Lee, B. J.; Lee, J. E.; Kwak, M. K.; Suh, K.-Y. Directional Oil Sliding Surfaces with Hierarchical Anisotropic Groove Microstructures. *Adv. Mater.* **2013**, *25*, 5756−5761.

(8) Long, J.; Fan, P.; Jiang, D.; Han, J.; Lin, Y.; Cai, M.; Zhang, H.; Zhong, M. Anisotropic Sliding of Water Droplets on the Superhydrophobic Surfaces with Anisotropic Groove-Like Micro/Nano Structures. *Adv. Mater. Interfaces* **2016**, *3*, 1600641.

(9) Lee, S. G.; Lim, H. S.; Lee, D. Y.; Kwak, D.; Cho, K. Tunable Anisotropic Wettability of Rice Leaf-Like Wavy Surfaces. *Adv. Funct. Mater.* **2013**, *23*, 547−553.

(10) Cheng, Z.; Zhang, D.; Lv, T.; Lai, H.; Zhang, E.; Kang, H.; Wang, Y.; Liu, P.; Liu, Y.; Du, Y.; Dou, S.; Jiang, L. Superhydrophobic Shape Memory Polymer Arrays with Switchable Isotropic/Anisotropic Wetting. *Adv. Funct. Mater.* **2018**, *28*, 1705002.

(11) Chatelin, R.; Poncet, P. A parametric study of mucociliary transport by numerical simulations of 3D non-homogeneous mucus. *J. Biomech.* **2016**, *49*, 1772−1780.

(12) Wheatley, D.; Wang, A. M.; Strugnell, G. E. Expression of primary cilia in mammalian cells. *Cell Biol. Int.* **1996**, *20*, 73−81.

(13) Hirokawa, N.; Tanaka, Y.; Okada, Y.; Takeda, S. Nodal flow and the generation of left-right asymmetry. *Cell* **2006**, *125*, 33−45.

(14) Keißner, A.; Brücker, C. Directional fluid transport along artificial ciliary surfaces with base-layer actuation of counter-rotating orbital beating patterns. *Soft Matter* **2012**, *8*, 5342−5349.

(15) Toonder, J. M. J. d.; Onck, P. R. Microfluidic manipulation with artificial/bioinspired cilia. *Trends Biotechnol.* **2013**, *31*, 85−91.

(16) Fahrni, F.; Prins, M. W. J.; van Ijzendoorn, L. J. Micro-fluidic actuation using magnetic artificial cilia. *Lab Chip* **2009**, *9*, 3413−3421.

(17) Khaderi, S. N.; Craus, C. B.; Hussong, J.; Schorr, N.; Belardi, J.; Westerweel, J.; Prucker, O.; Rühe, J.; den Toonder, J. M. J.; Onck, P. R. Magnetically-actuated artificial cilia for microfluidic propulsion. *Lab Chip* **2011**, *11*, 2002−2010.

(18) Glazer, P. J.; Leuven, J.; An, H.; Lemay, S. G.; Mendes, E. Multi-Stimuli Responsive Hydrogel Cilia. *Adv. Funct. Mater.* **2013**, *23*, 2964−2970.

(19) Ben, S.; Tai, J.; Ma, H.; Peng, Y.; Zhang, Y.; Tian, D.; Liu, K.; Jiang, L. Cilia-Inspired Flexible Arrays for Intelligent Transport of Viscoelastic Microspheres. *Adv. Funct. Mater.* **2018**, *28*, 1706666.

(20) Ben, S.; Zhou, T.; Ma, H.; Yao, J.; Ning, Y.; Tian, D.; Liu, K.; Jiang, L. Multifunctional Magnetocontrollable Superwettable-Microcilia Surface for Directional Droplet Manipulation. *Adv. Sci.* **2019**, *6*, 1900834.

(21) Cao, M.; Jin, X.; Peng, Y.; Yu, C.; Li, K.; Liu, K.; Jiang, L. Unidirectional Wetting Properties on Multi-Bioinspired Magnetocontrollable Slippery Microcilia. *Adv. Mater.* **2017**, *29*, 1606869.

(22) Dai, X.; Sun, N.; Nielsen, S. O.; Stogin, B. B.; Wang, J.; Yang, S.; Wong, T.-S. Hydrophilic Directional Slippery Rough Surfaces for Water Harvesting. *Sci. Adv.* **2018**, *4*, No. eaaq0919.

(23) Bixler, G. D.; Bhushan, B. Bioinspired rice leaf and butterfly wing surface structures combining shark skin and lotus effects. *Soft Matter* **2012**, *8*, 11271−11284.

(24) Feng, L.; Li, S.; Li, Y.; Li, H.; Zhang, L.; Zhai, J.; Song, Y.; Liu, B.; Jiang, L.; Zhu, D. Super-Hydrophobic Surfaces: From Natural to Artificial. *Adv. Mater.* **2002**, *14*, 1857−1860.

(25) Liu, J.; Guo, H.; Zhang, B.; Qiao, S.; Shao, M.; Zhang, X.; Feng, X.-Q.; Li, Q.; Song, Y.; Jiang, L.; Wang, J. Guided Self-Propelled Leaping of Droplets on a Micro-Anisotropic Superhydrophobic Surface. *Angew. Chem., Int. Ed.* **2016**, *55*, 4265−4269.

(26) Fang, Y.; Yong, J.; Chen, F.; Huo, J.; Yang, Q.; Zhang, J.; Hou, X. Bioinspired Fabrication of Bi/Tridirectionally Anisotropic Sliding Superhydrophobic PDMS Surfaces by Femtosecond Laser. *Adv. Mater. Interfaces* **2018**, *5*, 1701245.

(27) Kim, J. H.; Kang, S. M.; Lee, B. J.; Ko, H.; Bae, W.-G.; Suh, K. Y.; Kwak, M. K.; Jeong, H. E. Remote Manipulation of Droplets on a Flexible Magnetically Responsive Film. *Sci. Rep.* **2015**, *5*, 17843.

(28) Bixler, G. D.; Bhushan, B. Fluid drag reduction and efficient self-cleaning with rice leaf and butterfly wing bioinspired surfaces. *Nanoscale* **2013**, *5*, 7685−7710.

(29) Guo, P.; Wang, Z.; Heng, L.; Zhang, Y.; Wang, X.; Jiang, L. Magnetocontrollable Droplet and Bubble Manipulation on a Stable Amphibious Slippery Gel Surface. *Adv. Funct. Mater.* **2019**, *29*, 1808717.

(30) Huang, Y.; Stogin, B. B.; Sun, N.; Wang, J.; Yang, S.; Wong, T.-S. A Switchable Cross-Species Liquid Repellent Surface. *Adv. Mater.* **2017**, *29*, 1604641.

(31) Bai, X.; Yang, Q.; Fang, Y.; Zhang, J.; Yong, J.; Hou, X.; Chen, F. Superhydrophobicity-memory surfaces prepared by a femtosecond laser. *Chem. Eng. J.* **2020**, *383*, 123143.

(32) Sugioka, K.; Cheng, Y. Ultrafast lasers—reliable tools for advanced materials processing. *Light: Sci. Appl.* **2014**, *3*, No. e149. DOI: 10.1038/lsa.2014.30

(33) Malinauskas, M.; Zukauskas, A.; Hasegawa, S.; Hayasaki, Y.; Mizeikis, V.; Buividas, R.; Juodkazis, S. Ultrafast laser processing of materials: from science to industry. *Light: Sci. Appl.* **2016**, *5*, No. e16133. DOI: 10.1038/lsa.2016.133

(34) Zhu, Y.; Antao, D. S.; Xiao, R.; Wang, E. N. Real-Time Manipulation with Magnetically Tunable Structures. *Adv. Mater.* **2014**, *26*, 6442−6446.

(35) Yang, Z.; Park, J. K.; Kim, S. Magnetically Responsive Elastomer-Silicon Hybrid Surfaces for Fluid and Light Manipulation. *Small* **2018**, *14*, 1702839.

(36) Zhang, Q.; He, L.; Zhang, X.; Tian, D.; Jiang, L. Switchable Direction of Liquid Transport via an Anisotropic Microarray Surface and Thermal Stimuli. *ACS Nano* **2020**, *14*, 1436−1444.

(37) Zhang, Y.; Li, Y.; Hu, Y.; Zhu, X.; Huang, Y.; Zhang, Z.; Rao, S.; Hu, Z.; Qiu, W.; Wang, Y.; Li, G.; Yang, L.; Li, J.; Wu, D.; Huang, W.; Qiu, C.; Chu, J. Localized Self-Growth of Reconfigurable Architectures Induced by a Femtosecond Laser on a Shape-Memory Polymer. *Adv. Mater.* **2018**, *30*, 1803072.

(38) Zhang, Y.-L.; Chen, Q.-D.; Xia, H.; Sun, H.-B. Designable 3D nanofabrication by femtosecond laser direct writing. *Nano Today* **2010**, *5*, 435−448.

(39) Hu, Y.; Wang, Z.; Jin, D.; Zhang, C.; Sun, R.; Li, Z.; Hu, K.; Ni, J.; Cai, Z.; Pan, D.; Wang, X.; Zhu, W.; Li, J.; Wu, D.; Zhang, L.; Chu, J. Botanical-Inspired 4D Printing of Hydrogel at the Microscale. *Adv. Funct. Mater.* **2019**, *30*, 1907377.

(40) Jiang, S.; Hu, Y.; Wu, H.; Zhang, Y.; Zhang, Y.; Wang, Y.; Zhang, Y.; Zhu, W.; Li, J.; Wu, D.; Chu, J. Multifunctional Janus Microplates Arrays Actuated by Magnetic Fields for Water/Light Switches and Bio-Inspired Assimilatory Coloration. *Adv. Mater.* **2019**, *31*, 1807507.

(41) Tang, L.; Zeng, Z.; Wang, G.; Shen, L.; Zhu, L.; Zhang, Y.; Xue, Q. Study of Oil Dewetting Ability of Superhydrophilic and Underwater Superoleophobic Surfaces from Air to Water for High-Effective Self-Cleaning Surface Designing. *ACS Appl. Mater. Interfaces* **2019**, *11*, 18865−18875.

(42) Yong, J.; Chen, F.; Yang, Q.; Jiang, Z.; Hou, X. A Review of Femtosecond-Laser-Induced Underwater Superoleophobic Surfaces. *Adv. Mater. Interfaces* **2018**, *5*, 1701370.

(43) Lin, Y.; Hu, Z.; Zhang, M.; Xu, T.; Feng, S.; Jiang, L.; Zheng, Y. Magnetically Induced Low Adhesive Direction of Nano/Micropillar Arrays for Microdroplet Transport. *Adv. Funct. Mater.* **2018**, *28*, 1800163.